Available online at www.sciencedirect.com
SCIENCE DIRECT®
Journal of Magnetic Resonance 165 (2003) 260–264
JMR Journal of Magnetic Resonance
www.elsevier.com/locate/jmr

Probing magnetic fields on crystals of the nanomagnet Mn_{12}-acetate by electron paramagnetic resonance

B. Rakvin,[a] D. Žilić,[a] J.M. North,[b] and N.S. Dalal[b,*]

[a] *Ruder Bošković Institute, P.O. Box 180, 10002 Zagreb, Croatia*
[b] *Department of Chemistry and Biochemistry and National High Magnetic Field Laboratory, Florida State University, Tallahassee, FL 32306, USA*

Received 27 May 2003; revised 15 August 2003

Communicated by Arthur Schweiger

Abstract

We report on electron paramagnetic resonance (EPR) probing of magnetic fields and magnetic field gradients near the surface of a single crystal of the nanomagnet $[Mn_{12}O_{12}(CH_3COO)_{16}(H_2O)_4]\cdot 2CH_3COOH\cdot 4H_2O$ (Mn_{12}-Ac). As the EPR probe, we utilized a $0.7\,mm \times 30\,\mu m \times 30\,\mu m$ fiberous needle of the organic conductor *N*-methylphenazinium-tetracyanoquinodimethane (NMP-TCNQ), which yields an exceptionally sharp peak, with a 0.2 G ($\sim 20\,\mu T$) width. In the presence of Mn_{12}-Ac, the probe's peak exhibits splitting on temperature lowering, which depends on the orientation of the Zeeman field relative to the axis of easy magnetization of the employed Mn_{12}-Ac crystal. The shifted peaks yield the magnitude of the magnetic field from Mn_{12}-Ac crystal to which the various fibers of the probe are subjected. In conjunction with electron microscopy, the shifts yield the field gradient at the crystal surface and its change with temperature. For Mn_{12}-Ac at 10 K, the surface magnetic field was measured to be in the mT range and its gradient on the order of 50 T/m.

1. Introduction

Single molecule magnets (SMMs) have recently been the focus of considerable experimental and theoretical interest [1–3], since they were found to exhibit the novel phenomenon of quantum tunneling of the magnetization (QTM) [4,5]. A SMM is defined to be a compound in which essentially a single molecule can exhibit a hysteresis loop, hence the basis of memory storage at the molecular level [1–3], and possibly, quantum computation [6]. One of the most studied SMMs is $[Mn_{12}O_{12}(CH_3COO)_{16}(H_2O)_4]\cdot 2CH_3COOH\cdot 4H_2O$, henceforth Mn_{12}-Ac [4–28]. Mn_{12}-Ac exhibits a ground state spin $S = 10$, and an easy-axis anisotropy parameter $D = 0.46\,T$. The Mn_{12}-Ac system can thus be described as a double-well quantum system, with a large barrier height of $\sim DS^2 \approx 46\,T \approx 65\,K$, into which a spin 10 particle resides with energy levels labelled by the magnetic quantum number $m_s = \pm 10, \pm 9, \ldots, 0$. Magnetization measurements have established that below about 2 K, the magnetization of the $S = 10$ system undergoes reorientational transitions at a rate that becomes essentially temperature independent, implying that the reorientation occurs primarily via quantum tunneling of the magnetization vector across the potential barrier. Because of the implied overlap of the wavefunctions of the magnetization vector across the double-well, it has been recently suggested that Mn_{12}-Ac could form the basis of a quantum bit [6]. Mn_{12}-Ac has thus been well investigated by essentially all available techniques, including magnetization measurements of a.c. and d.c. susceptibility [4,5,7,8], electron paramagnetic resonance (EPR) [9–13], Raman spectroscopy [14,15], NMR [16–21], specific heat [22], infrared and optical techniques [23–25], neutron scattering [26,27], conductivity [28] and micro-Hall [28]. We here report a simple EPR-based method of measuring the surface magnetization or, equivalently, effective magnetic fields near an Mn_{12}-Ac crystal. It seems that such data would be useful if Mn_{12}-Ac were to be utilized as a device element.

* Corresponding author.
E-mail address: dalal@chem.fsu.edu (N.S. Dalal).

1090-7807/$ - see front matter © 2003 Elsevier Inc. All rights reserved.
doi:10.1016/j.jmr.2003.08.010

We utilize EPR spectroscopy as a technique, using a small (0.7 mm long, 30 μm × 30 μm diameter) needle of the organic charge transfer, conducting salt *N*-methyl-phenazium-tetracyanoquinodimethane (NMP-TCNQ). NMP-TCNQ was chosen because its EPR spectrum is perhaps the sharpest known single peak (with a peak to peak width, $\Delta B_{pp} \sim 0.2\,G \approx 20\,\mu T$), at a *g*-value around 2.0030. The peak position should thus be a sensitive probe of the presence of any magnetic field in its vicinity. Electron microscopy measurements (Fig. 1) show that the probe is fibrous, consisting of several discrete bundles. Thus if there are strong field gradients present near the crystal surface, the different bundles would be subject to different fields and hence the EPR peak should split into many components. A knowledge of the probe's fibrous structure would thus enable the determination of the magnetic field gradient over the probe's dimensions.

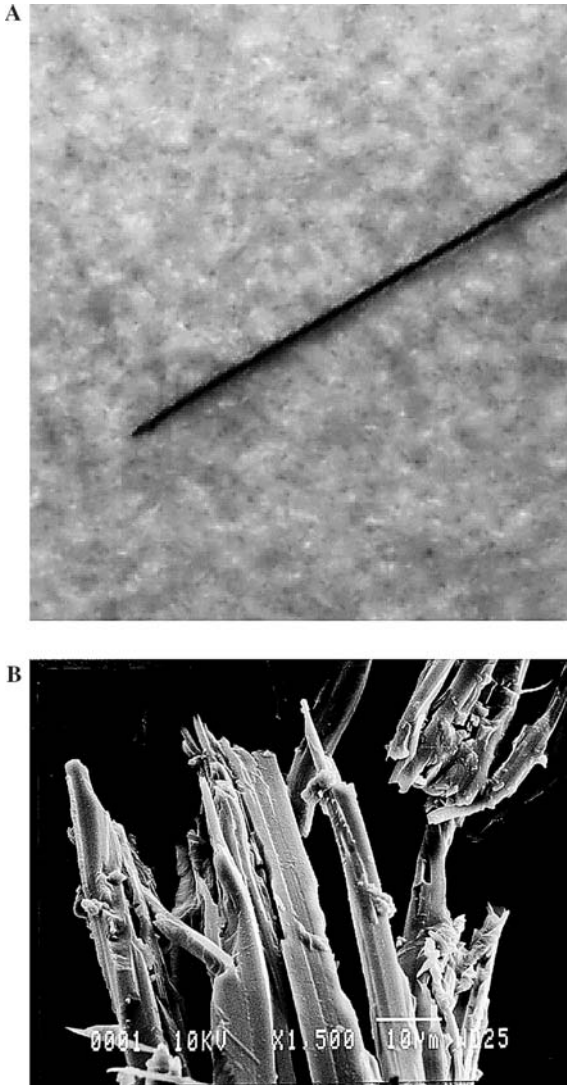

Fig. 1. (A) NMP-TCNQ probe shown under 60× magnification. (B) Scanning electron microscope image of the NMP-TCNQ probe at 1500× magnification.

Similar studies have been reported earlier. Smirnov et al. [29] used TCNQ as a paramagnetic probe at 140 GHz to measure the field gradient produced by ferromagnetic disks used in EPR imaging. Schultz and Gullikson [30] used DPPH to measure the d.c. magnetization of a sample with a conventional EPR spectrometer. Studies by Sueki et al. [31] monitored magnetic susceptibility effects on EPR spectra of polypyrrole on gold, palladium, platinum, and tungsten wire. Further studies of paramagnetic samples as field gradients are contained in a review edited by Eaton et al. [32].

2. Experimental procedure

2.1. Materials and EPR instrumentation

Single crystals of Mn_{12}-Ac were grown using Lis' procedure described earlier [33] and grew as rectangular rods in dimensions of a few mm^3, with the easy axis of magnetization being along the longest dimension. EPR measurements were carried out with a Bruker 580 FT/CW X-band EPR spectrometer equipped with standard Oxford Instruments model DTC2 temperature controller. All measurements were performed with magnetic-field modulation amplitude of 10 μT at 100 kHz. The microwave power level used was low (about 0.1 mW) in order to minimize power saturation and broadening of the probe's EPR signals.

2.2. NMP-TCNQ probe

NMP-TCNQ was prepared according to the literature [34,35]. This probe yields an intense, homogeneous, narrow EPR signal with a peak-to-peak linewidth, ΔB_{pp}, of about 20 μT over a wide temperature interval (from 295 down to 4 K). The probe used here was a small needle shaped sample ~0.7 mm long and ~30 μm × 30 μm in diameter (Fig. 1A). Upon higher magnification it can be seen that the needle shaped NMP-TCNQ sample consists of a bundle of several thinner needles as shown in Fig. 1B. When mounted on the crystal surface, the NMP-TCNQ needle yields an EPR peak whose position and lineshape are determined by an average of the applied Zeeman field and the local fields over the spatial extension of the needle. As can be noted from Fig. 2, the peak first broadened and then split as the temperature is lowered and the magnetic field produced by the SMM is increased.

The probe's signal shifted as the orientation of its needle axis relative to the Zeeman field direction and the Mn_{12}-Ac crystal's easy magnetization direction (*z*-axis) was changed, as can be noted in Fig. 3. This orientation is indicated for each measurement as an inset.

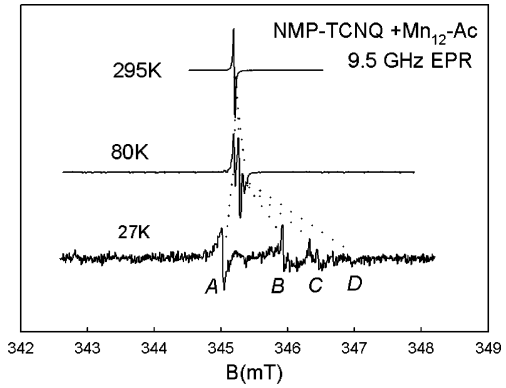

Fig. 2. Typical EPR spectra of the NMP-TCNQ probe deposited on the surface the Mn_{12}-Ac crystal at various temperatures. The easy axis of the Mn_{12}-Ac crystal is oriented along the magnetic Zeeman field.

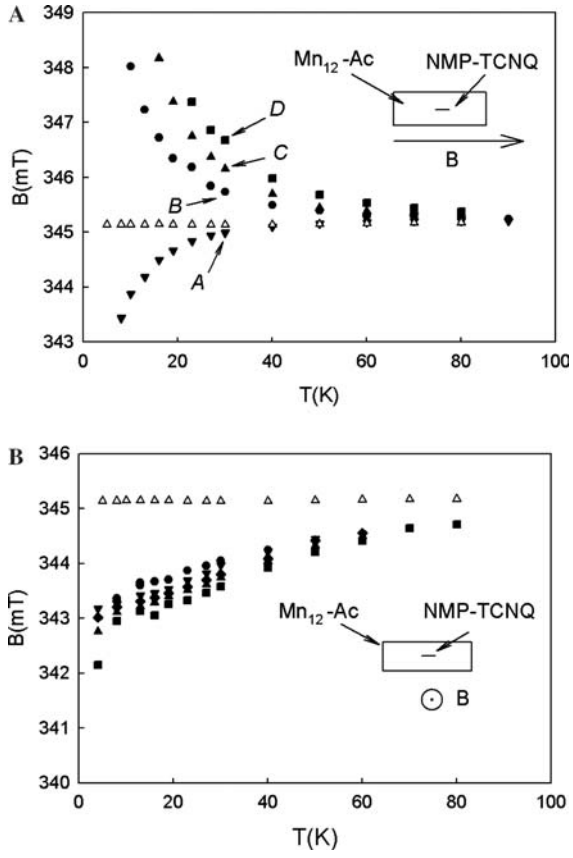

Fig. 3. Temperature dependencies of the shifted resonance fields for the NMP-TCNQ probe deposited on surface of SMM crystal (filled circles) and for the NMP-TCNQ probe itself (open triangles). The position of the probe on the crystal surface and orientation in magnetic field is denoted with small sketch in the corner of the each pictures A and B.

3. Results and discussion

Fig. 2 shows typical EPR spectra of the NMP-TCNQ probe at the Mn_{12}-Ac crystal surface at several temperatures. It is noted that at room temperature the EPR spectrum from the probe with Mn_{12}-Ac is slightly shifted ($\sim$30 μT) relative to its signal position in the absence of Mn_{12}-Ac. In the temperature interval of 295–100 K, the signal shows further shifts and slight broadening. Below 100 K, the signal is seen as several split lines, labelled A, B, C, and D, shifted from the room temperature signal. The spectra presented in Fig. 2 are for the Zeeman field, B, oriented along the easy (c-) axis of Mn_{12}-Ac with the probe's long axis also aligned along the same direction. Fig. 3 shows the temperature dependence of the lines shifts for the Zeeman field along and perpendicular to the easy axis. It should be mentioned that the signal from the probe itself (without Mn_{12}-Ac) also shifts slightly in the same temperature interval, but this shift is within the size of the symbol (open triangles) as presented in Fig. 3. As discussed below, it is significant that the shifts are to both the high-field and the low-field side of the probe's signal and the amount of shift depends on orientation and temperature. The observed resonance fields in Figs. 3A and B with two opposite splitting contributions can be described qualitatively inside the approximation of a point dipole–dipole coupling model [36] assuming that one dipole $\overrightarrow{\mu_1} = -g_1\beta\overrightarrow{S_1}$ corresponds to the NMP-TCNQ probe and another dipole $\overrightarrow{\mu_2}$ corresponds to the Mn_{12}-Ac crystal. The two moments have parallel principal axes. Taking that the shortest distance r is along the x axis, and the z axis is parallel to the needle shaped NMP-TCNQ crystal and the Mn_{12}-Ac crystal, as shown in Fig. 3, their interaction can be written in the form [36]

$$H_{12} = \beta r^{-3}(2g_{1x}\mu_{2x}S_{1x} - g_{1y}\mu_{2y}S_{1y} - g_{1z}\mu_{2z}S_{1z}). \quad (1)$$

The contribution of the local magnetic field due to the magnetic moment to the Zeeman magnetic field at resonance can now be described as:

$$H = \beta(g_{1x}B_xS_{1x} + g_{1y}B_yS_{1y} + g_{1z}B_zS_{1z}) + H_{12}, \quad (2)$$

$$= \beta[g_{1x}(B_x + 2\mu_{2x}r^{-3})S_{1x} + g_{1y}(B_y - \mu_{2y}r^{-3})S_{1y} + g_{1z}(B_z - \mu_{2z}r^{-3})S_{1z}], \quad (3)$$

$$= \beta[g_{1x}(B_x + \Delta B_x)S_{1x} + g_{1y}(B_y + \Delta B_y)S_{1y} + g_{1z}(B_z + \Delta B_z)S_{1z}]. \quad (4)$$

One can assume that by placing the needle shaped NMP-TCNQ on top of a crystal of Mn_{12}-Ac, the probe will experience an additional magnetic field ΔB along each component, as given in Eq. (4), due to magnetization of the Mn_{12}-Ac crystal. It is important to note that the Hamiltonian obtained in Eqs. (3) and (4) predicts opposite contributions of local magnetic fields, ΔB, to the Zeeman field along the distance r, and perpendicular to r as was observed experimentally. The effect of the angular dependence of the shifted probe's spectra can be discussed in terms of modified g-values of the probe. As expected, because of the macroscopic distance

between the probe and the Mn_{12}-Ac crystal, ΔB is much smaller than the Zeeman field B, hence the effect can be treated as a small perturbation and can be discussed also as an effective change in the probe's g-tensor. The solution of the spin Hamiltonian (2) without the contribution of the interaction part, H_{12} is straightforward and, in terms of the g-tensor value can be given as [36]:

$$g_1 = (g_{1x}^2 l^2 + g_{1y}^2 m^2 + g_{1z}^2 n^2)^{1/2}, \quad (5)$$

where (l, m, n) represent direction cosines of the orientation of the magnetic field in reference to the axis system. Taking into account the orientation around y with the magnetic field inside the xz plane and the corresponding angle, θ, between the direction of the magnetic field and the z axis, the g_1 is given in the form

$$g_1 = (g_{1\perp}^2 \sin^2\theta + g_{1\parallel}^2 \cos^2\theta)^{1/2}. \quad (6)$$

The complete spin Hamiltonian can be solved in terms of perturbation theory assuming a small contribution of the interaction part to the Zeeman spin Hamiltonian. In order to get the solution in the form of a g_{eff}-tensor value, one can employ the identity for the Zeeman energy transition $h\nu$ of the form

$$g_{1x}B_x = (g_{1x} - \Delta g_x)(B_x + \Delta B_x). \quad (7)$$

By employing relation (7), and the approximation that the term $\Delta g_x \Delta B_x$ is small and can be neglected, the spin Hamiltonian in (2)–(4) can be written in the form

$$H = \beta(g_{\text{eff}1x}B_x S_{1x} + g_{\text{eff}1y}B_y S_{1y} + g_{\text{eff}1z}B_z S_{1z}). \quad (8)$$

For the magnetic field orientation in the (x, z) plane, the g_{eff} value can be obtained in a similar fashion as in Eq. (7)

$$g_{\text{eff}1} = (g_{\text{eff}1\perp}^2 \sin^2\theta + g_{\text{eff}1\parallel}^2 \cos^2\theta)^{1/2} \quad (9)$$

Fig. 4 shows the angular variation of the g-value of the peak B, when the orientation of the Zeeman field is varied in the crystal ac (easy magnetization) plane. The data can be fitted to Eq. (9) shown as the continuous line in Fig. 4. The agreement is seen to be satisfactory, thus supporting our simple model.

Let us assume that the Zeeman field is parallel to the z axis and the resonance condition is obtained in the form

$$h\nu/\beta B_{\text{eff}\parallel} = g_{\text{eff}\parallel}, \quad (10)$$

where $B_{\text{eff}\parallel} = (B_\parallel + \Delta B_\parallel)$ includes the magnetic field shift due to the magnetization along the easy axis. Since $g_{\text{eff}\parallel}$ (2.0008) is smaller than g_{1z} (2.0030) as seen in Fig. 4, the $B_{\text{eff}\parallel}$ is larger than $B_\parallel$ leading to the positive contribution of the field shift due to magnetization along the easy axes ($\mu_{2\parallel}$). A direct support for this was additionally provided by our observation that over a wide temperature interval, from 300 to 20 K, the temperature dependence of the line shifts varied in proportion to the sample's magnetization as measured independently with a superconducting quantum interference device (SQUID) magnetometer. Fig. 5 shows a typical set of scaled magnetization and shift data for the external field oriented along the easy (z) axis; the proportionality of the field shifts to the magnetization is clearly evident. In addition, the increasing local magnetic field leads to an opposite sign of the defined magnetic moment $\vec{\mu_2}$. The same analysis provided for the perpendicular orientation supports the opposite magnetic field shift for $B_{\text{eff}\perp}$, as was experimentally detected. It should be reiterated that $\mu_{2\parallel}$ and $\mu_{2\perp}$ are only some effective magnetic moment components of the sample's dipolar field. These quantities can be measured accurately only if the distance of the probe from the crystal is known.

We can calculate the field gradient produced by a single Mn_{12}-Ac crystal. This can be obtained from the knowledge of the measured field shift as a function of the distance between the bundles in the probe, as measured via SEM. Thus the average gradient measured was estimated to be about 50 T/m.

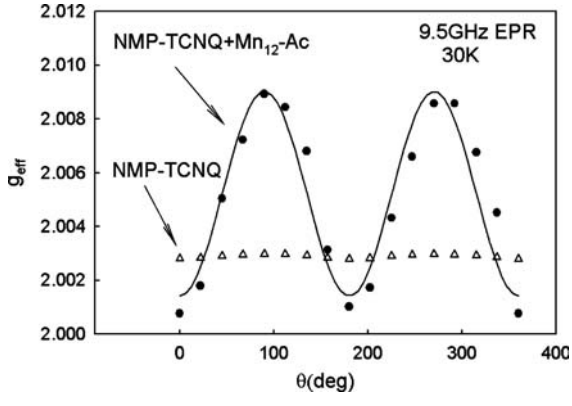

Fig. 4. Angular dependence of the g-tensor for peak B (Fig. 2) of the NMP-TCNQ probe deposited on the surface of SMM crystal (filled circles) and for the NMP-TCNQ probe itself (open triangles) detected at 30 K. The solid line represents the best-fitted line to experimental points calculated from Eq. (9). θ is the angle between the applied magnetic field and the z axis of the Mn_{12}-Ac crystal in the xz plane.

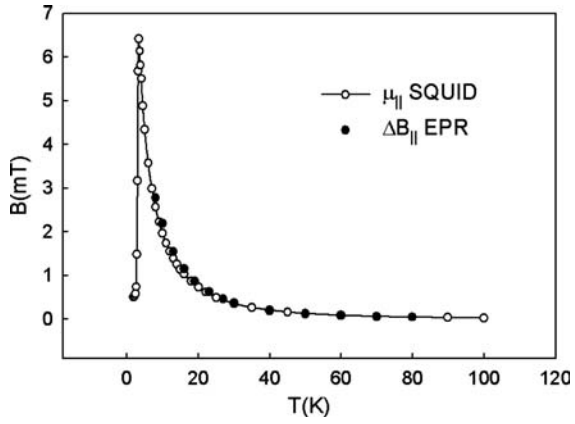

Fig. 5. Comparison of SQUID and EPR data. The open circles represent the scaled magnetization measured by a SQUID for the easy axis, while the solid circles are the shifts for peak B in Fig. 2.

4. Conclusions

The present investigation demonstrates the feasibility of measuring surface magnetization or equivalently, the magnetic fields at the surface of SMM nanomagnets by employing EPR measurements on a spin probe. While these results are preliminary, they seem to have potential for development into a fast, inexpensive, and easily available methodology for characterizing the surface magnetic properties of highly magnetic molecules. We acknowledge that the point dipole model is only an approximation. Further, more detailed numerical simulations are planned, and will be reported separately.

References

[1] D. Gatteschi, A. Caneschi, L. Pardi, R. Sessoli, Science 265 (1994) 1054.
[2] G. Christou, D. Gatteschi, D.N. Hendrickson, R. Sessoli, MRS Bull. 25 (2000) 66.
[3] E.M. Chudnovsky, J. Tejada, Macroscopic Quantum Tunneling of the Magnetic Moment, Cambridge University Press, Cambridge, UK, 1998.
[4] J.R. Friedman, M.P. Sarachik, J. Tejada, R. Ziolo, Phys. Rev. Lett. 76 (1996) 3830.
[5] L. Thomas, F. Lionti, R. Ballou, D. Gatteschi, R. Sessoli, B. Barbara, Nature 383 (1996) 145.
[6] M.N. Leuenberger, D. Loss, Nature (London) 410 (2001) 789.
[7] J.A.A.J. Perenboom, J.S. Brooks, S. Hill, T. Hathaway, N.S. Dalal, Phys. Rev. B 58 (1998) 330.
[8] R. Blinc, B. Zalar, A. Gregorvic, D. Arcon, Z. Kutnjak, C. Filipc, A. Levstik, R.M. Achey, N.S. Dalal, Phys. Rev. B 67 (2003) 094401.
[9] (a) S. Hill, J.A.A.J. Perenboom, N.S. Dalal, T. Hathaway, T. Stalcup, J.S. Brooks, Phys. Rev. Lett. 80 (1998) 2453;
(b) A.L. Barra, D. Gatteschi, R. Sessoli, Phys. Rev. B 56 (1997) 8192.
[10] R. Blinc, P. Cevc, D. Arcon, N.S. Dalal, R.M. Achey, Phys. Rev. B 63 (2001) 212401.
[11] K. Park, M.A. Novotny, N.S. Dalal, S. Hill, P.A. Rikvold, Phys. Rev. B 65 (2001) 014426.
[12] S. Hill, S. Maccagnano, K. Park, R.M. Achey, J.M. North, N.S. Dalal, Phys. Rev. B 65 (2002) 224410.
[13] K. Park, M.A. Novotny, N.S. Dalal, S. Hill, P.A. Rikvold, J. Appl. Phys. 91 (2002) 7167.
[14] J.M. North, L.J. van de Burgt, N.S. Dalal, Solid State Commun. 123 (2002) 75.
[15] J.M. North, R.M. Achey, N.S. Dalal, Phys. Rev. B 66 (2002) 174437.
[16] A. Lascialfari, Z.H. Jang, F. Borsa, P. Carretta, D. Gatteschi, Phys. Rev. Lett. 81 (1998) 3773.
[17] Y. Furukawa, K. Watanabe, K. Kumagai, Z.H. Jang, A. Lascialfari, F. Borsa, D. Gatteschi, Phys. Rev. B 62 (2000) 14246.
[18] R.M. Achey, P. Kuhns, A. Reyes, W. Moulton, N.S. Dalal, Polyhedron 20 (2001) 1745;
Phys. Rev. B 64 (2001) 064420;
Solid State Commun. 121 (2002) 107.
[19] T. Goto, T. Kudo, T. Koshida, Y. Fujii, A. Oyamada, J. Arai, K. Takeda, K. Awaga, Phys. B 1227 (2000) 284.
[20] Y. Furukawa, K. Watanabe, K. Kumagai, F. Borsa, D. Gatteschi, Phys. Rev. B 64 (2001) 104401.
[21] T. Kubo, T. Goto, T. Koshiba, K. Takeda, K. Awaga, Phys. Rev. B 65 (2002) 224425.
[22] A.M. Gomes, M.A. Novak, R. Sessoli, A. Caneschi, D. Gatteschi, Phys. Rev. B 57 (1998) 5021.
[23] S.M. Oppenheimer, A.B. Sushkov, J.L. Musfeldt, R.M. Achey, N.S. Dalal, Phys. Rev. B 65 (2002) 054419.
[24] A.B. Sushkov, B. Jones, J.L. Musfeldt, R.M. Achey, N.S. Dalal, Phys. Rev. B 63 (2001) 214408.
[25] A.B. Sushkov, J.L. Musfeldt, Y.J. Wang, R.M. Achey, N.S. Dalal, Phys. Rev. B 66 (2002) 144430.
[26] M. Hennion, L. Pardi, I. Mirebeau, E. Suard, R. Sessoli, A. Caneschi, Phys. Rev. B 56 (1997) 8819.
[27] I. Mirebeau, M. Hennion, H. Casalta, H. Anders, H.U. Gudel, A.V. Ivadova, A. Caneschi, Phys. Rev. Lett. 83 (1999) 628.
[28] (a) J.M. North, D. Zipse, N.S. Dalal, E.S. Choi, E. Jobiliong, J.S. Brooks, D.L. Eaton, Phys. Rev. B 67 (2003) 174407;
(b) L. Bockacheva, A.D. Kent, M.A. Walters, Phys. Rev. Lett. 85 (2000) 4803;
K.M. Mertes, Y. Suzuki, M.P. Sarachik, Y. Paltiel, H. Shtrikman, E. Zeldov, E.M. Rumberger, D.N. Hendrickson, G. Christou, Phys. Rev. B 65 (2002) 212401.
[29] A.I. Smirnov, O.G. Poluectov, Y.S. Lebedev, J. Mag. Res. 97 (1992) 1.
[30] S. Schultz, E.M. Gullikson, Rev. Sci. Instrum. 54 (1983) 1383.
[31] M. Sueki, S.S. Eaton, G.R. Eaton, J. Mag. Res. A 105 (1993) 25.
[32] Y.S. Lebedev, O.Y. Yamichenko, Localized Gradients, in: G.R. Eaton, S.S. Eaton, K. Ohno (Eds.), EPR Imaging and In Vivo EPR, CRC Press, Boca Raton, 1991, pp. 25–34.
[33] T. Lis, Acta Crystallogr. Sect. B 36 (1980) 2042.
[34] B. Rakvin, M. Požek, A. Dulčić, Phys. C 170 (1990) 166.
[35] A.I. Vistnes, L.R. Dalton, J. Mag. Res. 54 (1983) 78.
[36] A. Abragam, B. Bleaney, Electron Paramagnetic Resonance of Transition Ions, Dover Publications, New York, NY, 1970, 492.
[37] N.M. Atherton, Electron Spin Resonance Theory on Applications, John Wiley, New York, 1973, 189.